

Oxidation of Cymantrene Analogues of Ferrocifen: Electrochemical, Spectroscopic, and Computational Studies of the Parent Complex 1,1'-Diphenyl-2-cymantrenylbutene

Kan Wu,[†] Ji Young Park,[‡] Rachael Al-Saadon,[§] Hyerim Nam,^{‡,||,∇} Yujin Lee,^{‡,||,∇} Siden Top,[⊥] Gérard Jaouen,^{⊥,#} Mu-Hyun Baik,^{*,‡,||} and William E. Geiger^{*,†}

[†]Department of Chemistry, University of Vermont, Burlington, Vermont 05405, United States

[‡]Center for Catalytic Hydrocarbon Functionalizations, Institute for Basic Science (IBS), Daejeon 34141, South Korea

[§]Department of Chemistry, Duke University, Durham, North Carolina 27708, United States

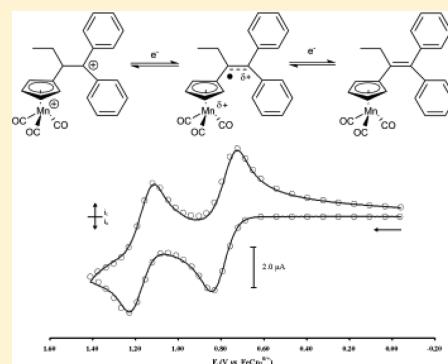
^{||}Department of Chemistry, Korea Advanced Institute of Science and Technology (KAIST), Daejeon 34141, South Korea

[⊥]Sorbonne Université, UPMC, CNRS, Institut Parisien de Chimie Moléculaire (IPCM), UMR 8232, 4 place Jussieu, 75005 Paris, France

[#]PSL, Chimie ParisTech, 11 rue Pierre and Marie Curie, F-75005 Paris, France

Supporting Information

ABSTRACT: The oxidative electrochemical behavior of 1,1'-diphenyl-2-cymantrenylbutene (**1**), a cymantrene analogue of the breast cancer drug ferrocifen, was shown to involve the sequential electron-transfer series $1/1^+/1^{2+}$ in dichloromethane/0.05 M $[\text{NBu}_4][\text{B}(\text{C}_6\text{F}_5)_4]$ ($E_{1/2}$ values 0.78 and 1.18 V vs ferrocene). By a combination of spectroscopic and computational techniques, it was shown that the cymantrene functionality plays an important role in dissipating the positive charges in the oxidized compounds and is therefore an active participant in the redox events. The redox-active orbital goes from roughly equal degrees of organometallic and π -organic (diphenylolefin) makeup in **1** to increasingly organic based fractions in 1^+ and 1^{2+} . Structural changes mimicking those of oxidized tetrakis(aryl)ethylenes accompany the one-electron oxidations. There is sufficient unpaired electron density on the manganese center in 1^+ to allow for oxidatively induced ligand exchange of one or more of the carbonyl ligands with donor ligands, including phosphites and pyridine. The complex $\text{Mn}(\text{CO})_2\text{P}(\text{OPh})_3(\eta^5\text{-C}_5\text{H}_4(\text{Et})\text{C}=\text{C}(\text{C}_6\text{H}_5)_2)$ was prepared by the “electrochemical switch” method, wherein $[\text{Mn}(\text{CO})_2\text{P}(\text{OPh})_3(\eta^5\text{-C}_5\text{H}_4(\text{Et})\text{C}=\text{C}(\text{C}_6\text{H}_5)_2)]^+$, produced by the oxidation of **1** in the presence of $\text{P}(\text{OPh})_3$, was reduced back to the neutral CO-substituted complex.



INTRODUCTION

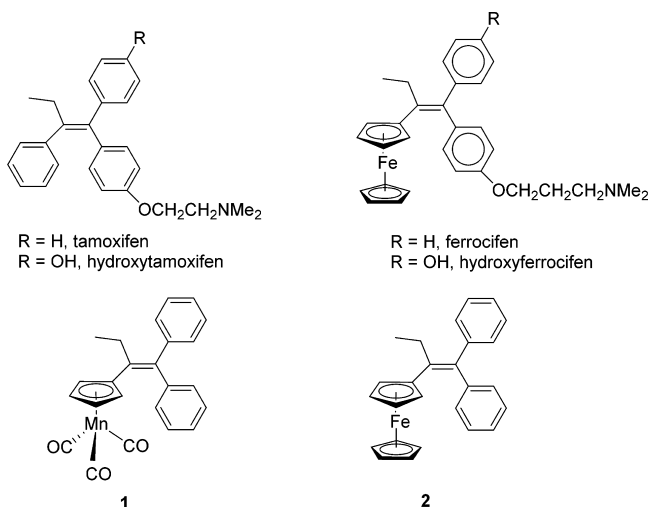
Modeled in part on the structure of the breast cancer drug tamoxifen (Scheme 1),^{1–3} a large number of ferrocenyl-derivatized diaryl butenes have been tested for activity against cancer cells.^{4,5} Several of these “ferrocifen mimics” show promising antiproliferative activity against both estrogen receptor-positive and receptor-negative cell lines.⁵ Replacing the phenyl group of tamoxifen by the ferrocenyl group increases the lipophilicity, and perhaps more importantly, facilitates its one-electron oxidation. Ruthenium and osmium analogues of ferrocifen are less cytotoxic to breast cancer cell lines, a factor attributed to the higher M(II)/M(III) redox potentials of the heavier homologues.^{5,6}

Less widely studied are analogues in which the organometallic unit has a half-sandwich structure. Here we describe the oxidation of the cyclopentadienylmanganese tricarbonyl (cymantrene) derivative **1**, which may be seen as the parent of a class of group 5 organometallic diarylbutenes. Although compound **1** shows only weak antiproliferative action against breast cancer cell lines,⁷ other cymantrenyl-labeled poly(aryl) butenes exhibit significant

activity.^{8,9} An unexplored aspect of the cymantrenyl-tagged compounds is that dramatic changes in the redox potential and other properties of **1** may be obtained with derivatives in which one or more carbonyl group is replaced by an electron-donating ligand.¹⁰ For example, the $E_{1/2}$ value of the one-electron oxidation of $\text{MnCp}(\text{CO})_2(\text{PPh}_3)$ is 650 mV negative of that of $\text{MnCp}(\text{CO})_3$,^{11,12} and even greater shifts are possible with double substitution of the CO ligands.¹³ To better understand these systems, we prepared several diaryl butenes substituted at the 2-butenyl position with cyclopentadienylmanganese tricarbonyl groups and investigated their oxidative redox properties. The communication describing our preliminary experimental findings on **1**¹⁴ is supplemented in the present paper by calculations giving information on the electronic and molecular structures of **1** and its oxidation products, 1^+ and 1^{2+} . We also describe the oxidatively induced substitution of carbonyl groups

Received: March 29, 2018

Scheme 1



in **1** by donor ligands and report the $E_{1/2}$ potentials of the resulting carbonyl-substituted complexes.

The potential redox activity of organometallic-tagged tamoxifen-type compounds is not restricted to the organometallic unit. In fact, the 1,1'-diarylethylene position of these molecules is expected to be redox-active, on the basis of the fact that most poly(aryl)-ethylenes undergo two chemically reversible oxidations at accessible potentials. For example, in dichloromethane/0.1 M $[\text{NBu}_4][\text{PF}_6]$, tetraanisylethylene is converted to its radical cation and dication at 0.41 and 0.53 V vs ferrocene (FcH), respectively.^{15–18} Oxidation potentials of the diaryldiethyl analogue 3,4-bis-(anisyl)-3-hexene are only slightly more positive.¹⁷ More recent papers on tetraarylethylene redox chemistry are available.^{18–20} Consistent with the expectation that a ferrocenyl group should be easier to oxidize than a diarylethylene group, the first oxidations of 1,1'-diphenyl-2-ferrocenylbutene (**2**) and other members of the ferrocifen family give monocations that have essentially ferrocenium (Fe(III)) character.^{21–23} In contrast, oxidation of the manganese center in **1** is expected to be more difficult than oxidation of the diarylethylene group, on the basis of the fact that $E_{1/2}$ for the oxidation of cymantrene is 0.91 V vs FcH.²⁴ Thus, radical cations of the type 1^+ might be expected to have spin and charge that is highly localized in the diarylethylene (π -ligand) part of the molecule. In fact, as we show by both experiment and calculation, the HOMO of the parent complex **1**, as well as the SOMO of 1^+ , has similar amounts of organometallic and π -organic character. It is of practical importance to obtain a measure of the metal vs π -ligand makeup of these systems owing to the fact that delocalization between the organometallic group and the diarylethylene group is thought to facilitate the follow-up reactions of positively charged ferrocifen derivatives that exhibit strong biological activity.^{5,21–23} Furthermore, it has been shown that the degree of metal–ligand charge delocalization in a cymantrene-type radical cation affects the rates of carbonyl substitution reactions for the $\text{Mn}(\text{CO})_3$ group.²⁵

The present study was simplified by the fact that the anodic electron-transfer reactions of **1** are not complicated by the types of follow-up reactions that would be expected if the aryl moieties in **1** contain hydroxyl or other groups that are subject to oxidative activation. A separate study has been carried out on the *p*-hydroxyl- and *p*-methoxy-substituted analogues of **1**, and those results will be reported in a separate paper.

EXPERIMENTAL DETAILS

All operations were carried out under nitrogen or argon using either Schlenk or drybox techniques. Solvents were dried and purified either by refluxing them in drying agents or by passing them down an alumina column under argon. Infrared spectra were obtained on either an IRFT BOMEM Michelson-100 spectrometer or an ATI-Mattson Infinity Series FTIR instrument operating at a resolution of 4 cm^{-1} . In situ IR spectroelectrochemistry was carried out with a Remspec, Inc., fiber-optic system using a methodology previously described.²⁶ ^1H and ^{13}C NMR spectra were obtained with Bruker spectrometers, and mass spectra were obtained with a Neromag R 10-10C unit using chemical ionization. EPR spectra were obtained with a Bruker ESP 300E spectrometer. $[\text{NBu}_4][\text{B}(\text{C}_6\text{F}_5)_4]$ was recrystallized from dichloromethane/diethyl ether after being prepared by metathesis of $[\text{NBu}_4]\text{Br}$ and $\text{K}[\text{B}(\text{C}_6\text{F}_5)_4]$.²⁷

Synthesis of $\text{Mn}(\text{CO})_3(\eta^5\text{-C}_5\text{H}_4)(\text{Et})\text{C}=\text{C}(\text{C}_6\text{H}_5)_2$ (1**).** TiCl_4 (1.1 g, 6.0 mmol) was added dropwise to a suspension of zinc powder (0.78 g, 12.0 mmol) in 20 mL THF at 0°C . A blue mixture was obtained, which was refluxed for 2 h, whereupon the solution became black. The reaction medium was allowed to come to room temperature, after which a solution of benzophenone (0.73 g, 4.0 mmol) and propionylcymantrene²⁸ (0.52 g, 2.0 mmol) in 10 mL of THF was added dropwise. The resulting mixture was refluxed for 4 h, after which it was cooled to room temperature and then poured into 100 mL of water and acidified to pH 1 with a diluted aqueous HCl solution. After the solution was extracted by dichloromethane ($3 \times 50\text{ mL}$) and washed with 50 mL of water, the solvent was evaporated, leaving 1.17 g of crude product that was chromatographed on a silica gel column with 1/50 diethyl ether/petroleum ether as eluent, giving 0.38 g (46%) of the desired product. It was recrystallized from diethyl ether/pentane, giving yellow crystals with mp 102°C . ^1H NMR (300 MHz, d_6 -acetone): δ 7.39–7.17 (m, 10H, aromatic rings), 4.77 (t, $J = 2.1\text{ Hz}$, 2H, C_3H_4), 4.62 (t, $J = 2.1\text{ Hz}$, 2H, C_3H_4), 2.31 (q, 2H, $J = 7.5\text{ Hz}$, CH_2CH_3), 1.08 (t, 3H, $J = 7.5\text{ Hz}$, CH_2CH_3). ^{13}C NMR (75.5 MHz, d_6 -acetone): δ 15.4 (CH_3), 28.5 (CH_2), 82.8 and 85.7 (CH, C_3H_4), 105.1 (C_{ip} , C_5H_4), 127.7, 129.3, 129.4, 129.5, and 130.1 (CH_{arom}), 132.9, 143.7, 144.2, and 144.4 (C_q of two C_6H_4 and $\text{C}=\text{C}$). IR (CH_2Cl_2): ν_{CO} 2017 and 1932 cm^{-1} . MS (CI): m/z 411 $[\text{MH}]^+$; 326 $[\text{M} - 3\text{CO}]^+$. Anal. Calcd for $\text{C}_{24}\text{H}_{19}\text{O}_3\text{Mn}$: C, 70.25, H, 4.67. Found: C, 69.75, H, 4.55.

Synthesis of $\text{Mn}(\text{CO})_2\text{P}(\text{OPh})_3(\eta^5\text{-C}_5\text{H}_4)(\text{Et})\text{C}=\text{C}(\text{C}_6\text{H}_5)_2$. A 32 mL portion of a $\text{CH}_2\text{Cl}_2/0.05\text{ M}$ $[\text{NBu}_4][\text{B}(\text{C}_6\text{F}_5)_4]$ solution that was 3.04 mM in **1** (40 mg) and 4.5 mM in $\text{P}(\text{OPh})_3$ (44 mg) was placed in the working compartment of a three-compartment electrochemical cell. With application of an applied potential of 1.0 V vs ferrocene to a platinum-basket electrode, the solution was electrolyzed for 30 min, at which time 1.0 F had been passed and the solution had changed color from its original pale yellow to pink. After CV scans were obtained which showed that **1** had been quantitatively converted to $[\text{Mn}(\text{CO})_2\text{P}(\text{OPh})_3(\eta^5\text{-C}_5\text{H}_4)(\text{Et})\text{C}=\text{C}(\text{C}_6\text{H}_5)_2]^+$ ($E_{1/2} = 0.46\text{ V}$), the applied potential at the platinum basket was changed to 0.1 V. This initiated the reduction of the phosphite-substituted cation and resulted in passage of 0.85 F as the solution went from pink to green. The working compartment solution was evaporated while being protected from light. A pentane extract of the crude product was evaporated to dryness, and the resulting yellow solid was spotted on an alumina column with dichloromethane and eluted with diethyl ether. The yellow band trailing the unreacted triphenyl phosphite was evaporated, giving 27 mg (40%) of a yellow powder that was identified as $\text{Mn}(\text{CO})_2\text{P}(\text{OPh})_3(\eta^5\text{-C}_5\text{H}_4)(\text{Et})\text{C}=\text{C}(\text{C}_6\text{H}_5)_2$ on the basis of its IR spectrum (ν_{CO} 1956, 1893 cm^{-1} in CH_2Cl_2) and the fact that the potential of its reversible oxidation ($E_{1/2} = 0.46\text{ V}$) matched that obtained from cyclic voltammetry scans when **1** was oxidized in the presence of triphenyl phosphite (see Results and Discussion).

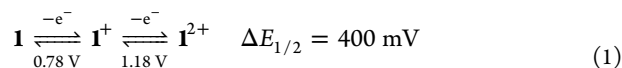
Electrochemistry. Voltammetry was carried on with a three-electrode format, using a Pt wire for the auxiliary electrode and a homemade Ag/AgCl electrode for the experimental reference electrode. The latter consisted of a AgCl-coated silver wire that was immersed in a solution of 0.05 M $[\text{NBu}_4][\text{B}(\text{C}_6\text{F}_5)_4]$ in dichloromethane which was separated from the working electrode compartment by a fine-porosity

glass frit. The potentials in this paper are all referenced to the ferrocene/ferrocenium couple,²⁹ the potential of which was obtained by the in situ method³⁰ at an appropriate point in the experiment. Working electrodes for voltammetry measurements were 1 or 2 mm glassy-carbon disks obtained from Bioanalytical Systems and polished before use with Buehler diamond paste. A platinum-basket working electrode was used in a three-compartment H cell for bulk electrolysis. The potentiostat was a PARC Model 273 instrument interfaced to a computer controlled by homemade software. The temperature of the electrolyte solution was controlled to within 1 °C by a TFS Flexi-Cool system. In general, the electrochemical procedures followed those described in an earlier paper.²⁴ Well-known diagnostics³¹ were applied to cyclic voltammetry measurements at different scan rates to check for diffusion control and chemical and electrochemical reversibility of the redox couples. Digital simulations were carried out using Digisim 3.0 (Bioanalytical Systems) on background-subtracted cyclic voltammograms.

Computational Methods. All calculations were performed at the B3LYP-D3³² level of density functional theory implemented in the Q-Chem 4.4 package.³³ For geometry optimizations, the 6-31G** level basis set³⁴ was used for all main-group elements and Mn was represented using the Los Alamos LANL2DZ basis set,³⁵ which is a double- ζ quality basis set including effective core potentials. Convergence to local minima was confirmed by vibrational frequency calculations that showed no imaginary frequency. The energies of these species were re-evaluated using the cc-pVTZ³⁶ basis set for main-group elements and LANL2DZ for Mn. This is a well-established and thoroughly tested protocol for calculating redox potentials³⁷ and modeling redox processes. Solvation energy corrections were obtained using a continuum solvation model (c-pcm) employing the double- ζ basis set, and zero-point vibrational energy and entropy corrections were obtained also using the double- ζ basis set. The dielectric constant of dichloromethane was set to 9.08 at room temperature.³⁸ Vibrational frequencies computed using the harmonic oscillator model at the B3LYP/double- ζ level of theory were scaled by a factor of 0.9613.³⁹ Cartesian coordinates of all computed structures are given in the Supporting Information. The percent orbital contributions for fragments were obtained using the Chemisian⁴⁰ program.

RESULTS AND DISCUSSION

Oxidation of 1. Electrochemical studies of the anodic reactions of **1** were carried out in dichloromethane, using either [NBu₄][PF₆] or [NBu₄][B(C₆F₅)₄] as the supporting electrolyte. Owing to the fact that a single cyclic voltammetry (CV) scan through the first oxidation wave resulted in severe electrode fouling in [PF₆]⁻-based electrolyte, the electrochemical work reported in this paper was carried out in [B(C₆F₅)₄]⁻-based electrolyte, the use of which circumvented adsorption problems and gave reproducible voltammograms at glassy-carbon electrodes. Positive-going CV scans of the parent compound **1** showed two reversible one-electron oxidations at $E_{1/2}(1) = 0.78$ V and $E_{1/2}(2) = 1.18$ V vs FeCp₂^{0/+}. That the two reactions are diffusion-controlled, quasi-Nernstian processes (see electron-transfer series in eq 1) was confirmed by evaluation of the standard CV diagnostic criteria³¹ and by digital simulations (Figure 1). The latter was used to determine the diffusion coefficient of **1** as 1.5×10^{-5} cm² s⁻¹ at 298 K. Both **1**⁺ and **1**²⁺ are stable on the electrolysis time scale and were characterized by spectroscopic methods.



Spectral Characterization of Oxidation Products. To more broadly characterize the oxidation products, the monocation and dication of **1** were generated by bulk anodic electrolysis at 273 K. Electrolysis at $E_{\text{appl}} = 0.9$ V consumed 1.0 F, giving complete conversion to the monocation **1**⁺, as shown by linear scan voltammetry. Continuation of the electrolysis at $E_{\text{appl}} = 1.3$ V

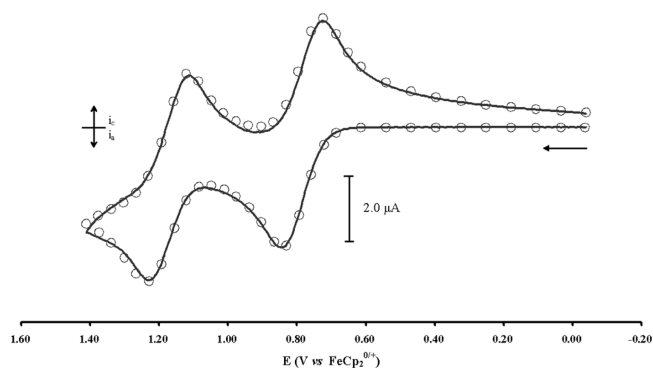


Figure 1. Experimental (solid line) and simulated (circles) CVs of 1.25 mM **1** in CH₂Cl₂/0.05 M [NBu₄][B(C₆F₅)₄] at 298 K and 0.2 V s⁻¹ on a 1 mm glassy-carbon electrode.

consumed an additional 1.0 F and produced the dication **1**²⁺ in high yield. Cathodic re-electrolysis at $E_{\text{appl}} = 0$ V regenerated over 90% of the neutral starting material. The favorable stabilities of the oxidation products facilitated their spectral characterization. Carbonyl-region IR spectra were obtained either by the in situ fiber-optic method²⁷ or by simple transfer of an electrolysis sample to a solution IR cell. Examples of in situ spectra are shown in Figures 2 and 3 for the stepwise conversion of **1** to **1**⁺ and of **1**⁺ to **1**²⁺, respectively.

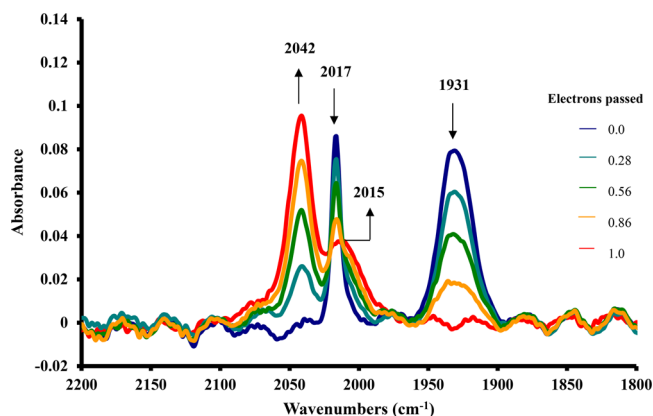


Figure 2. Fiber-optic IR spectra of solutions of 1.5 mM **1** in CH₂Cl₂/0.05 M [NBu₄][B(C₆F₅)₄] as the bulk oxidation proceeded at 273 K to 1 F passed, with $E_{\text{appl}} = 0.9$ V.

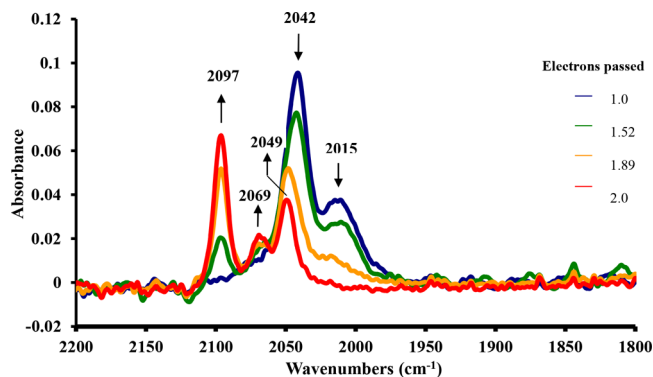


Figure 3. Fiber-optic IR spectra of 1.5 mM **1** in CH₂Cl₂/0.05 M [NBu₄][B(C₆F₅)₄] as the bulk oxidation proceeded at 273 K from 1 F passed to 2 F passed, with $E_{\text{appl}} = 1.3$ V.

It is well-known that metal–carbonyl stretching frequencies increase with increasing positive charge at the metal center as

Table 1. Summary of Metal–CO IR Absorptions for **1**, **1**⁺, and **1**²⁺ in CH₂Cl₂/0.05 M [NBu₄][TFAB] at 273 K^a

compound	exptl				DFT calcd			
	ν_{sym}	ν_{asym}	$\langle\nu_{\text{CO}}\rangle^b$	$\Delta\langle\nu_{\text{CO}}\rangle^c$	ν_{sym}	ν_{asym}	$\langle\nu_{\text{CO}}\rangle^b$	$\Delta\langle\nu_{\text{CO}}\rangle^c$
MnCp(CO) ₃	2022	1934	1963		2035	1979	1998	
[MnCp(CO) ₃] ⁺	2118	2058	2078	+115	2197	1959, 2085	2080	+82
1	2017	1931	1960		2028	1969, 1978	1991	
1 ⁺	2042	2015	2024	+64	2056	2015, 2024	2032	+41
1 ²⁺	2097	2049, 2069	2072	+112	2104	1989, 2075	2080	+89

^aData on MnCp(CO)₃^{0/+} (298 K) were taken from reference 24. ^b $\langle\nu_{\text{CO}}\rangle$ (cm⁻¹) = (ν_{sym} + $2\nu_{\text{asym}}$)/3. ^cAverage value referenced to neutral compound in cm⁻¹.

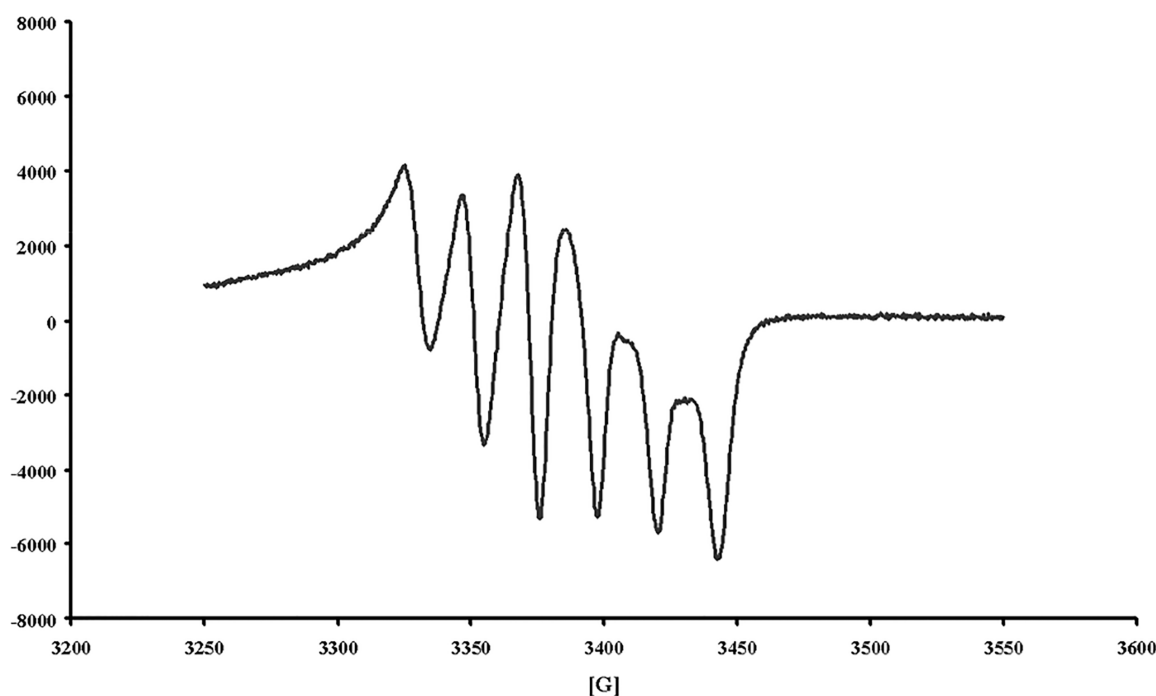


Figure 4. EPR spectrum of **1**⁺ at 77 K. The sample was prepared by exhaustive electrolysis of **1** in CH₂Cl₂/0.05 M [NBu₄][B(C₆F₅)₄] at 253 K, with $E_{\text{appl}} = 0.9$ V.

back-donation of electron density from the metal to the carbonyl π^* orbital is reduced, resulting in a stronger C–O bond.^{41–45} In the present case, it is informative to compare the increases in the average carbonyl stretching frequencies for **1**⁺ and **1**²⁺ with those observed for the oxidation of cymantrene itself²⁴ (see Table 1). Note that we use a *weighted* average of the three carbonyl absorption frequencies, counting the asymmetric stretch twice for compounds in which the two asymmetric ν_{CO} bands are not resolved. This analysis shows that removal of *two* electrons from **1** is required to produce the same degree of spectral shift (+112 cm⁻¹) as that seen with removal of a *single* electron from cymantrene (+115 cm⁻¹). In concert, the average increase in ν_{CO} (+64 cm⁻¹) for the monocation **1**⁺ is only slightly more than half of that observed for the cymantrene radical cation. We have also computed the vibrational frequencies using DFT calculations, and the results are convincingly similar, although in that case the computed energy shifts are slightly smaller. Calculations confirm that, to reproduce the frequency shift calculated for the oxidation of cymantrene (+82 cm⁻¹), *two* electrons must be removed from **1** to give a calculated shift of +89 cm⁻¹ in **1**²⁺. Significant fractions of the positive charges are thus seen to reside on the diphenylethynyl segment as electrons are removed from the molecule.

The rich contribution of the diphenylethynyl moiety to the SOMO is also indicated by the EPR spectrum of **1**⁺, which is not

characteristic of a highly metal centered Mn(II) system. The frozen-solution spectrum of **1**⁺, shown in Figure 4, is nearly isotropic, with $\langle g \rangle \approx 2.01$ and $A(^{55}\text{Mn})$ ($I = 5/2$) hyperfine splitting (hfs) of approximately 21 G. These features are in stark contrast to those reported for [MnCp(CO)₃]⁺, which has a highly anisotropic g value and an average Mn hfs of 70 G.²⁴

Calculations: Structures and Redox-Active Orbitals. The DFT-optimized structures of **1**, **1**⁺, and **1**²⁺ (Figure 5) reveal how electron removal affects the molecular structures of this series of redox-active molecules. In the neutral species **1**, the double bond between C2 and C3 is intact at a bond length of 1.358 Å, which is slightly longer than the value (~1.33 Å) typically seen in simple olefins.⁴⁶ The dihedral angle (C1–C2–C3–C4) of 167° is a bit distorted from that of an ideal planar geometry. Both deviations from an idealized olefin structure are due to the steric demands of the substituents in this tetrasubstituted olefin. The fact that the C2–C3 bond lengthened by ~0.06 Å to 1.422 Å in **1**⁺ is a consequence of removal of olefin π character, an effect that is enhanced with removal of the second electron. The resulting C2–C3 bond length of 1.489 Å in **1**²⁺ begins to approach that of a standard C–C single bond. Decreases in the dihedral angle from the 167° of **1** to 146° in **1**⁺ and then to 127° in **1**²⁺ are also consistent with a decreasing degree of double-bond character for C2–C3 as electrons are removed.

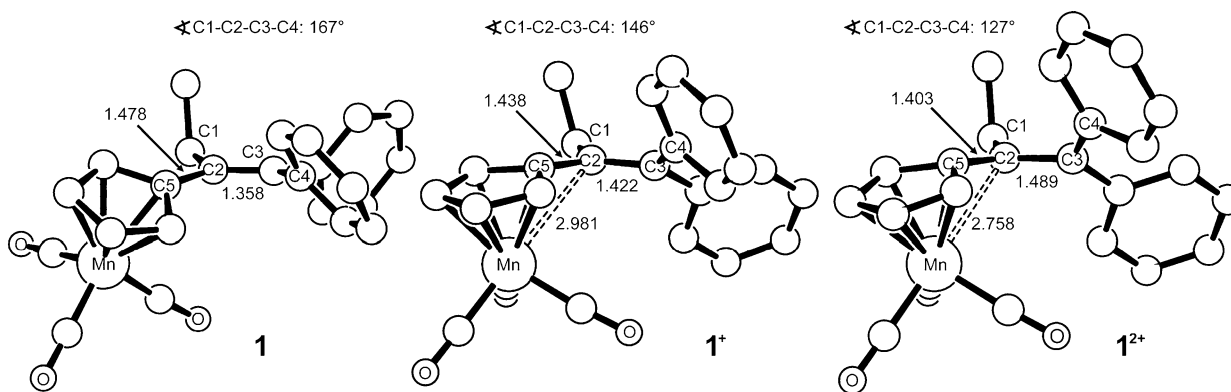


Figure 5. Optimized structures of **1**, **1⁺**, and **1²⁺**. Bond lengths are given in Å.

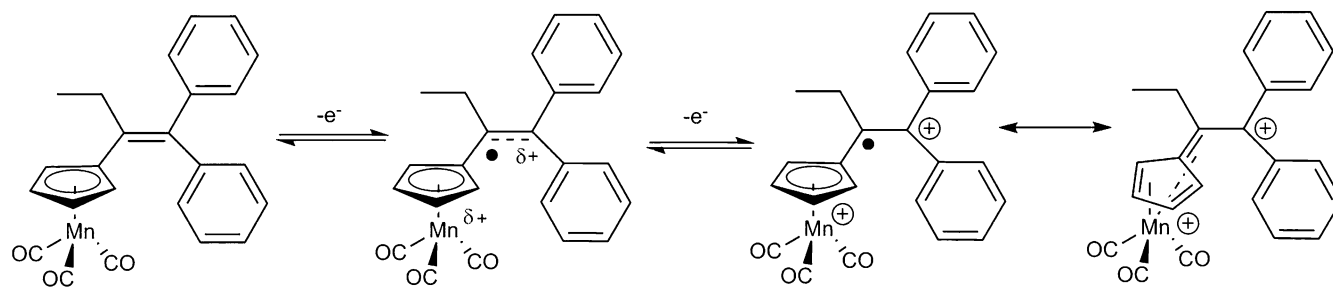


Figure 6. Representative structures of **1**, **1⁺**, and **1²⁺**.

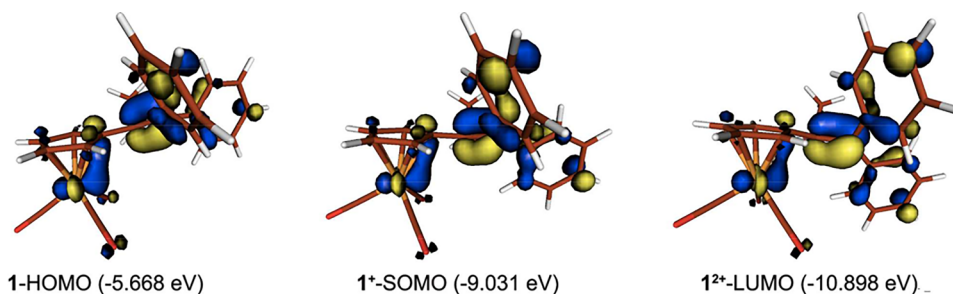


Figure 7. Redox-active orbitals of **1**, **1⁺**, and **1²⁺**. The isodensity value for the surface plots was set to 0.05 au.

The calculations also show that there is a significant change in the nature of the metal–ligand bonding as electrons are removed from **1**. There is a notable shortening of the C2–C5 distance from 1.478 to 1.438 and 1.403 Å in **1**, **1⁺**, and **1²⁺**, respectively, consistent with the progress toward a fulvene-type tautomer as the oxidation proceeds. The newly formed quasi-olefinic C2–C5 fragment can then engage the Mn center. The Mn–C1 distance in **1** is 3.231 Å, indicating that there is no electronic interaction between these atoms in the neutral complex. As oxidation introduces fulvene character to the ligand and a partial double bond is formed between C2 and C5, the Mn–C2 distance shortens to 2.981 Å and finally to 2.758 Å in **1⁺** and **1²⁺**, respectively. The structural features of the dication are highly reminiscent of the $[\text{Mn}(\text{CO})_3(\eta^4:\eta^2\text{-diphenylfulvene})]^+$ structure observed previously by Gleiter.^{47,48} A schematic illustration of the interplay between the electronic and molecular structures of the electron-transfer series is shown in Figure 6.

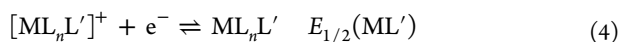
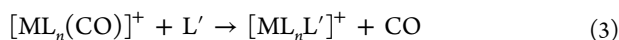
More detailed information about the frontier orbitals of the three members of the electron-transfer series are obtained from examination of Figure 7. To understand the origin of the electron removed during oxidation, we divided **1** into four different fragments: Mn, cyclopentadienyl ring (Cp), carbonyls, and the

1-ethyl-2-diphenylethene (olefin) moiety. By inspecting the atomic orbital contribution of these fragments to the redox-active orbital, we can obtain the percent contribution of each fragment. The HOMO of **1**, found at an energy of -5.668 eV, has about 2:1 ratio of π -ligand and organometallic character (33% $\text{Mn}(\text{C}_5\text{H}_4)(\text{CO})_3$). Specifically, the HOMO of **1** consists of 13% Mn, 13% Cp, 6% CO, and 67% olefin. The SOMO of **1⁺** shows a nearly identical distribution of 15, 12, 5, and 68%, respectively. This composition of the redox-active orbitals stands in stark contrast to the SOMO of the $[\text{MnCp}(\text{CO})_3]^+$ complex, which is formed by mixing 73% Mn, 9% Cp, and 18% CO based fragment orbitals. The redox-active orbital in **1** is derived from the interaction of the alkenyl π -MO with the nonbonding $d(xy)$ orbital of the low-spin Mn(I) d^6 center that is aligned parallel to the cyclopentadienyl plane. Removal of an electron from the HOMO of **1** leads to a substantial lowering of all orbital energies, with the singly occupied **1⁺**-SOMO being found at an electronic energy of -9.031 eV. Because the contributions of the organometallic fragment in **1**-HOMO and **1⁺**-SOMO are essentially the same, as illustrated in Figure 7, the orbital shapes remain nearly identical, despite the somewhat severe changes in geometrical structure described above. Removal of the unpaired electron associated with **1⁺**-SOMO

completes the oxidation and the resulting 94%-ligand based LUMO of I^{2+} is found at an energy of -10.898 eV.

The spectroscopic and computational data are in agreement that the stepwise oxidation of **1** involves orbitals which are *delocalized* between the cymantrenyl and diphenylethylenyl parts of the molecule and that the redox orbital becomes more π -ligand based as the oxidation proceeds from the neutral complex to the corresponding dication.

Redox-Switched Metal–Carbonyl Substitution. The fact that the radical cation I^+ contains significant cymantrenyl radical character suggests that the manganese carbonyl center should be susceptible to associative-driven CO substitution reactions.^{11,25,49–53} It is possible to take advantage of redox-dependent substitution rates in order to prepare CO-substituted complexes having metals in either the 17-electron or 18-electron electronic configurations under mild conditions. The “electrochemical switch” method outlined in eqs 2–4 shows how this might be carried out for a hypothetical metal complex $ML_n(CO)$. In this sequence, the neutral metal carbonyl complex is anodically oxidized to its radical cation (eq 2), which reacts with L' , producing the radical cation of the substitution product (eq 3). Owing to the fact that L' is invariably a stronger donor than CO, the potential $E_{1/2}(ML')$ is less positive than $E_{1/2}(MCO)$, assuring that the substitution product $[ML_nL']^+$ remains in the positively charged state as the electrolysis proceeds. $[ML_nL']^+$ may then be cathodically reduced to give the desired neutral substitution product (eq 4), which is then extracted from the electrolyte solution. A literature example of this process is the preparation of $Cr(\eta^6-C_6H_6)(CO)_2PPh_3$ from $Cr(\eta^6-C_6H_6)(CO)_3$.⁵⁴



Application of the electrochemical switch method to the preparation of the triphenyl phosphite complex $Mn(CO)_2P(OPh)_3(\eta^5-C_5H_4(Et)C=C(C_6H_5)_2)$ followed the expected protocol. Figure 8 shows a CV scan of **1** when a slight excess

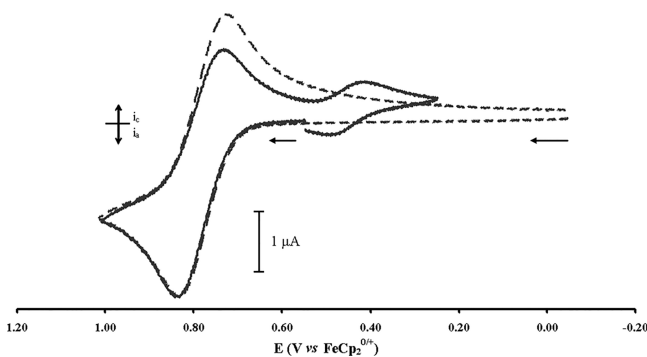


Figure 8. CVs of 1.0 mM **1** in the absence (dashed line) and the presence (solid line) of 1.5 mM $P(OPh)_3$ in $CH_2Cl_2/0.05$ M $[NBu_4][B(C_6F_5)_4]$ at 298 K and 0.2 V s^{-1} , with a 1 mm GCE.

of $P(OPh)_3$ is added to the solution. A reduction in the chemical reversibility of the $I^{0/+}$ couple is noted by comparing the scans taken before (dashed line) and after (solid line) addition of triphenyl phosphite. The follow-up product is seen to have a reversible reduction at $E_{1/2} = 0.46$ V, consistent with the replacement of a single CO by $P(OPh)_3$ in **1**. The $E_{1/2}$ shift of 0.32 V from that of $I^{0/+}$ is somewhat less than the average of 0.40 V observed for the

$P(OPh)_3$ for CO shifts in the cymantrene series $Mn(\eta^5-C_5H_4R(CO)_3)$ ($R = H, Me, I, CHO$),²⁵ most likely reflecting the increased charge delocalization in I^+ . A triphenyl phosphite substitution rate of 4.7×10^2 $M^{-1} s^{-1}$ was determined for I^+ by digital simulation, about an order of magnitude slower than that reported for the cymantrene radical cation.²⁵

Bulk anodic electrolysis ($E_{app} = 0.9$ V) of **1** in the presence of $P(OPh)_3$ released 1 F of charge and gave a single product showing a reversible wave at $E_{1/2} = 0.46$ V for the reduction of the CO-substituted cation $[Mn(CO)_2P(OPh)_3(\eta^5-C_5H_4(Et)C=C(C_6H_5)_2)]^+$. Changing E_{app} to 0.2 V required 1 F of charge and resulted in efficient conversion to neutral $Mn(CO)_2P(OPh)_3(\eta^5-C_5H_4(Et)C=C(C_6H_5)_2)$. This sequence can be followed in Figure 9. The dotted line was recorded before

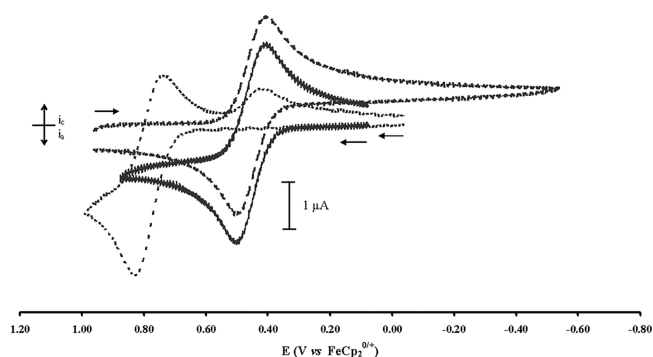


Figure 9. CVs of 1.0 mM **1** in the presence of 1.5 mM $P(OPh)_3$ in $CH_2Cl_2/0.05$ M $[NBu_4][B(C_6F_5)_4]$ before (dotted line) and after (dashed line) bulk oxidation at $E_{app} = 0.9$ V and after bulk reduction (solid line) at $E_{app} = 0.2$ V at 253 K and 0.2 V s^{-1} , with a 1 mm GCE.

beginning the anodic electrolysis and is analogous to the solid line in Figure 8. After completion of the electrolysis, the only electroactive compound in solution is the radical cation of the substitution product, responsible for the reversible cathodic wave at 0.46 V (dashed line). The solid line was recorded after completion of the cathodic “back-electrolysis” and arises from the reversible oxidation of the neutral substitution product $Mn(CO)_2P(OPh)_3(\eta^5-C_5H_4(Et)C=C(C_6H_5)_2)$. Comparison of the currents before and after the double electrolysis suggested that the in situ yield of $Mn(CO)_2P(OPh)_3(\eta^5-C_5H_4(Et)C=C(C_6H_5)_2)$ was greater than 80%.⁵⁵ As described in Experimental Details, workup of the electrochemically switched solution allowed isolation of the product, identified by its IR spectrum (Figure S1 in the Supporting Information) in 40% (unoptimized) yield.

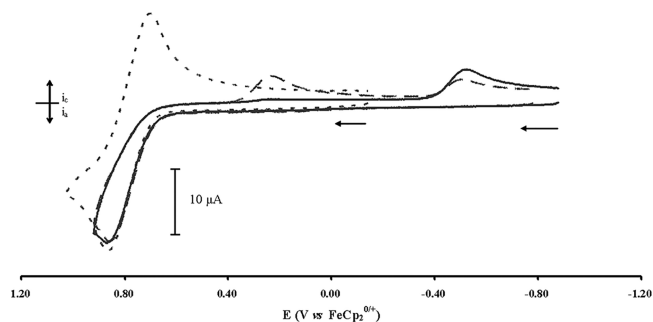


Figure 10. CVs of 0.90 mM **1** in the absence (dotted line) and the presence of 0.54 mM (long dashed line) and 2.70 mM (solid line) $P(O^iPr)_3$ in $CH_2Cl_2/0.05$ M $[NBu_4][B(C_6F_5)_4]$ at 253 K and 0.2 V s^{-1} , with a 3 mm GCE.

Table 2. Potentials vs Ferrocene in CH₂Cl₂/0.05 M [NBu₄][B(C₆F₅)₄] for the First Oxidation of Mn(CO)_{3–n}L_n(η⁵-C₅H₄(Et)C=C(C₆H₅)₂)

ligand (L)	<i>n</i>	<i>E</i> _{1/2} (V)	total shift from <i>E</i> _{1/2} of 1 (V)	<i>E</i> _L (cym)	<i>E</i> _L (lit)	comment
CO	0	0.78	n.a.	0.99	0.99 ^a	
P(OPh) ₃	1	0.46	–0.32	0.67	0.62 ^b	
P(O ⁱ Pr) ₃	1	0.25	–0.53	0.46		literature n.a.
P(OMe) ₃	1	0.24	–0.54	0.45	0.42 ^a	
P(ⁿ Bu)(OEt) ₂	1	0.24	–0.54	0.45		literature n.a.
pyridine	1	–0.21	–0.99	0	0.25 ^a	
P(OMe) ₃	2	–0.31	–1.09			additional shift of –0.55 V from <i>n</i> = 1
P(ⁿ Bu)(OEt) ₂	2	–0.52	–1.30			additional shift of –0.76 V from <i>n</i> = 1
P(O ⁱ Pr) ₃	2	–0.53	–1.31			additional shift of –0.78 V from <i>n</i> = 1

^aReference 57. ^bReference 25.

In the case of three phosphites having cone angles smaller than that of P(OPh)₃, examples of multiple CO substitutions were observed. An example is shown in Figure 10, which gives the CVs of **1** in the presence of two different concentrations of P(OⁱPr)₃. At a substoichiometric concentration of the phosphite (long dashed line), product waves are seen at *E*_{1/2} values of 0.25 and –0.49 V, which we attribute to the monosubstituted and disubstituted, [Mn(CO)_{3–n}[P(OⁱPr)₃]_n(η⁵-C₅H₄(Et)C=C(C₆H₅)₂)]⁺, *n* = 1 and 2, respectively. With excess P(OⁱPr)₃ (solid line), only the more negative wave for the disubstituted product is observed.

Assignments of the new waves to *n* = 1 or *n* = 2 substitution products were made on the basis of the expected shifts of the *E*_{1/2} values from that (0.78 V) of the first oxidation of the tricarbonyl parent compound **1**. Predictions of the shifts are possible for two phosphites, for which the so-called “ligand electronic parameter” has been reported.⁵⁷ This parameter was originally given as *E*_L on the basis of the oxidation of Cr(CO)₅L complexes.⁵⁷ In concert with the slightly different shifts in *E*_{1/2} values that have been observed for Mn(π-C₅H₄R)(CO)₂L complexes,^{11,25,58} we use the symbol *E*_L(cym) for the ligand electronic parameter of the cymantrene family of complexes, including **1**. As shown in Table 2, the *E*_L(cym) values determined for P(OPh)₃ and P(OMe)₃ match well with those reported in previous literature, confirming the assignments of the mono-CO-substituted products. The similarity of the *E*_L(cym) values for P(OⁱPr)₃ and P(ⁿBu)(OEt)₂ to that of P(OMe)₃ suggests that these three ligands have essentially the same donor strengths.

The CV curves assigned to the second CO substitution products for L = P(OMe)₃, P(OⁱPr)₃, and P(ⁿBu)(OEt)₂ are again shifted to potentials more negative than those observed for the singly substituted products. The sequential shifts are essentially identical for the L = P(OMe)₃ system, for which the oxidation goes smoothly from 0.78 to 0.24 and –0.31 V as *n* increases from 0 to 2 in Mn(CO)_{3–n}(P(OMe)₃)_n(η⁵-C₅H₄(Et)C=C(C₆H₅)₂). Somewhat larger shifts (ca. –0.77 V) for the apparent *n* = 2 products are seen for the other small phosphites, in comparison to values of only –0.45 V for the first substitution products. We cannot rule out the possibility that the more highly substituted products for L = P(OMe)₃ or P(OⁱPr)₃ are trisubstituted, but we think it more likely that the somewhat irregular shifts arise from electronic effects.

Redox-switched pyridine for CO substitution on the CV time scale was also observed for **1**, as indicated in Figure 11, although the reaction was not completed in that case. The *E*_{1/2} value of the pyridine substitution product (–0.21 V) is shifted positively by 0.99 V in comparison to the 0/+ potential of the tricarbonyl complex. IR spectra of a solution taken after a “redox switched” electrolysis had bands at ~1930 and 1845 cm^{–1} attributable to

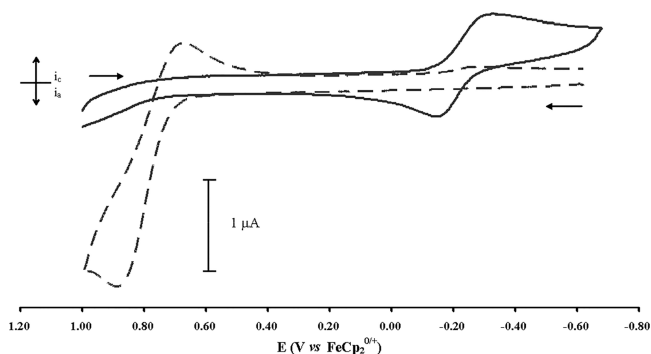


Figure 11. CVs (0.2 V s^{–1}, 1 mm GCE) of 0.9 mM **1** in the presence of 2.7 mM pyridine before (dashed line) and after (solid line) bulk oxidation (*E*_{appl} = 0.9 V) in CH₂Cl₂/0.05 M [NBu₄][B(C₆F₅)₄] at 253 K.

the Mn(CO)₂(pyridine) group (1933 and 1865 cm^{–1} reported for MnCp(CO)₂(py))⁵⁹ but also showed bands for considerable unsubstituted material (Figure S2 in the Supporting Information). The *E*_L(cym) value of zero determined for L = pyridine (vide infra) is somewhat larger than its reported *E*_L value (0.25).⁵⁷

The above data show that, by substitution of one or more carbonyl groups by donor ligands, the oxidation potential of Mn(CO)_{3–n}L_n(η⁵-C₅H₄(Et)C=C(C₆H₅)₂) can be altered by 1 V or more, allowing the possibility of generating a family of compounds that is either easier or more difficult to oxidize than their ferrocenyl analogues.

CONCLUSIONS

On the basis of the known differences in oxidative redox potentials among cymantrene, ferrocene, and the diphenylethylene moieties, the observation that the first oxidation of **1** occurs at a potential much higher (0.78 V) than that of the ferrocenyl analogue **2** (~0 V)^{21,56} was expected. Interestingly, however, this process involves loss of an electron from a HOMO orbital of **1** that is highly delocalized over the entire organometallic/π-organic framework, leading to a well-distributed sharing of positive charge in the monocation **1**⁺. There is sufficient positive charge at the Mn(CO)₃ group of **1**⁺ to facilitate the rapid substitution of one or more CO ligands by donor ligands, including several phosphites and pyridine. The resulting CO-substituted compounds have much milder oxidation potentials, in some cases being easier to oxidize than **2**. The fact that the SOMO of the radical cation **1**⁺ has mixed organometallic/π-organic character and the finding that the fraction of positive charge on the organic segment increases as electrons are removed will be helpful in

understanding both the follow-up reactions and the thermodynamic potential shifts that accompany the oxidations of analogues having more reactive groups in the phenyl rings.¹⁴ Electrochemical and computational studies of the *p*-hydroxy and *p*-methoxy derivatives of **1** will be detailed in a separate paper.

■ ASSOCIATED CONTENT

Supporting Information

The Supporting Information is available free of charge on the ACS Publications website at DOI: 10.1021/acs.organomet.8b00186.

IR spectra and xyz coordinates (PDF)

Cartesian coordinates for calculated structures (XYZ)

■ AUTHOR INFORMATION

Corresponding Authors

*E-mail for M.-H.B.: mbaik2805@kaist.ac.kr.

*E-mail for W.E.G.: William.Geiger@uvm.edu.

ORCID

William E. Geiger: 0000-0002-9152-8550

Present Address

[†]Samsung Electronics, Suwon 16677, South Korea.

Notes

The authors declare no competing financial interest.

■ ACKNOWLEDGMENTS

M.-H.B. acknowledges support from the Institute for Basic Science (IBS-R10-D1) in Korea. W.E.G. acknowledges support from the National Science Foundation (CHE-1212339 and CHE-1565441).

■ REFERENCES

- (1) (a) Jordan, V. C. *J. Med. Chem.* **2003**, *46*, 883–908. (b) Jordan, V. C. *J. Med. Chem.* **2003**, *46*, 1081–1111. (c) Jordan, V. C. *J. Natl. Cancer Inst.* **2014**, *106* (11), dju296.
- (2) Wu, X.; Hawse, J. R.; Subramaniam, M.; Goetz, M. P.; Ingle, J. N.; Spelsberg, T. C. *Cancer Res.* **2009**, *69*, 1722–1727.
- (3) Relevance of Breast Cancer Hormone Receptors and other Factors to the Efficacy of Adjuvant Tamoxifen: Patient-level Meta-analysis of Randomised Trials *Lancet* **2011**, *378*, 771–784.
- (4) Vessièrès, A.; Top, S.; Beck, W.; Hillard, E. A.; Jaouen, G. *Dalton Trans.* **2006**, 529–541.
- (5) Jaouen, G.; Vessièrès, A.; Top, S. *Chem. Soc. Rev.* **2015**, *44*, 8802–8817 and references therein.
- (6) Lee, H. Z. S.; Buriez, O.; Chau, F.; Labbé, E.; Ganguly, R.; Amatore, C.; Jaouen, G.; Vessièrès, A.; Leong, W. K.; Top, S. *Eur. J. Inorg. Chem.* **2015**, *2015*, 4217–4226.
- (7) Hillard, E. A.; Vessièrès, A.; Top, S.; Pigeon, P.; Kowalski, K.; Huché, Jaouen, G. *J. Organomet. Chem.* **2007**, *692*, 1315–1326.
- (8) Dallagi, T.; Saidi, M.; Jaouen, G.; Top, S. *Appl. Organomet. Chem.* **2013**, *27*, 28–35.
- (9) Dallagi, T.; Saidi, M.; Vessièrès, A.; Huché, M.; Jaouen, G.; Top, S. *J. Organomet. Chem.* **2013**, *734*, 69–77.
- (10) Connelly, N. G.; Geiger, W. E. *Adv. Organomet. Chem.* **1984**, *23*, 1–93.
- (11) Kochi, J. K. *J. Organomet. Chem.* **1986**, *300*, 139–166.
- (12) Atwood, C. G.; Bitterwolf, T. E.; Geiger, W. E. *J. Electroanal. Chem.* **1995**, *397*, 279–285.
- (13) Pike, R. D.; Rieger, A. L.; Rieger, P. H. *J. Chem. Soc., Faraday Trans. 1* **1989**, *85*, 3913–3925.
- (14) Wu, K.; Top, S.; Hillard, E. A.; Jaouen, G.; Geiger, W. E. *Chem. Commun.* **2011**, *47*, 10109–10111.
- (15) Phelps, J.; Bard, A. J. *J. Electroanal. Chem. Interfacial Electrochem.* **1976**, *68*, 313–335.

(16) Aalstad, B.; Parker, V. D. *J. Electroanal. Chem. Interfacial Electrochem.* **1982**, *136*, 251–258.

(17) Rathore, R.; Lindeman, S. V.; Kumar, A. S.; Kochi, J. K. *J. Am. Chem. Soc.* **1998**, *120*, 6931–6939.

(18) Schreivogel, A.; Maurer, J.; Winter, R.; Baro, A.; Laschat, S. *Eur. J. Org. Chem.* **2006**, *2006*, 3395–3404. The potentials in this paper are reported vs ferrocene/ferrocenium. Values reported vs other reference electrodes (see refs 15–18) would give similar potentials on conversion to the ferrocene reference.

(19) Talipov, M. R.; Boddada, A.; Hossain, M. M.; Rathore, R. *J. Phys. Org. Chem.* **2016**, *29*, 227–233.

(20) Mori, T.; Inoue, Y. *J. Phys. Chem. A* **2005**, *109*, 2728–2740.

(21) (a) Hillard, E.; Vessièrès, A.; Thouin, L.; Jaouen, G.; Amatore, C. *Angew. Chem., Int. Ed.* **2006**, *45*, 285–290. (b) Messina, P.; Labbé, E.; Buriez, O.; Hillard, E. A.; Vessièrès, A.; Hamels, D.; Top, S.; Jaouen, G.; Frapart, Y. M.; Mansuy, D.; Amatore, C. *Chem. - Eur. J.* **2012**, *18*, 6581–6587.

(22) Tan, Y. L. K.; Pigeon, P.; Hillard, E. A.; Top, S.; Plamont, M.-A.; Vessièrès, A.; McGlinchey, M. J.; Müller-Bunz, H.; Jaouen, G. *Dalton Trans.* **2009**, 10871–10881.

(23) Hillard, E.; Vessièrès, A.; Le Bideau, F.; Plaz, D.; Spera, D.; Huché, M.; Jaouen, G. *ChemMedChem* **2006**, *1*, 551–559.

(24) Laws, D. R.; Chong, D.; Nash, K.; Rheingold, A. L.; Geiger, W. E. *J. Am. Chem. Soc.* **2008**, *130*, 9859–9870.

(25) Wu, K.; Laws, D. R.; Nafady, A.; Geiger, W. E. *J. Inorg. Organomet. Polym. Mater.* **2014**, *24*, 137–144.

(26) Shaw, M. J.; Geiger, W. *Organometallics* **1996**, *15*, 13–15.

(27) LeSuer, R. J.; Buttolph, C.; Geiger, W. E. *Anal. Chem.* **2004**, *76*, 6395–6401.

(28) Fischer, E. O.; Fellman, W. *J. Organomet. Chem.* **1963**, *1*, 191–199.

(29) (a) Gritzner, G.; Kuta, J. *Pure Appl. Chem.* **1984**, *56*, 461–466. (b) Connelly, N. G.; Geiger, W. E. *Chem. Rev.* **1996**, *96*, 877–910.

(30) Gagne, R. E.; Koval, C. A.; Lisensky, G. C. *Inorg. Chem.* **1980**, *19*, 2854–2855.

(31) (a) Bard, A. J.; Faulkner, L. R. *Electrochemical Methods*, 2nd ed.; Wiley: New York, 2001; Chapter 6. (b) Geiger, W. E. In *Laboratory Techniques in Electroanalytical Chemistry*, 2nd ed.; Kissinger, P. T., Heineman, W. R., Eds.; Marcel Dekker: New York, 1996; Chapter 23.

(32) (a) Becke, A. D. *J. Chem. Phys.* **1993**, *98*, 1372. (b) Grimme, S.; Antony, J.; Ehrlich, S.; Krieg, H. *J. Chem. Phys.* **2010**, *132*, 154104.

(33) Shao, Y.; Gan, Z.; Epifanovsky, E.; Gilbert, A. T. B.; Wormit, M.; Kussmann, J.; Lange, A. W.; Behn, A.; Deng, J.; Feng, X.; Ghosh, D.; Goldey, M.; Horn, P. R.; Jacobson, L. D.; Kaliman, I.; Khaliullin, R. Z.; Kus, T.; Landau, A.; Liu, J.; Proynov, E. I.; Rhee, Y. M.; Richard, R. M.; Rohrdanz, M. A.; Steele, R. P.; Sundstrom, E. J.; Woodcock, H. L.; Zimmerman, P. M.; Zuev, D.; Albrecht, B.; Alguire, E.; Austin, B.; Beran, G. J. O.; Bernard, Y. A.; Berquist, E.; Brandhorst, K.; Bravaya, K. B.; Brown, S. T.; Casanova, D.; Chang, C.-M.; Chen, Y.; Chien, S. H.; Closser, K. D.; Crittenden, D. L.; Diedenhofen, M.; DiStasio, R. A.; Do, H.; Dutoi, A. D.; Edgar, R. G.; Fatehi, S.; Fusti-Molnar, L.; Ghysels, A.; Golubeva-Zadorozhnaya, A.; Gomes, J.; Hanson-Heine, M. W. D.; Harbach, P. H. P.; Hauser, A. W.; Hohenstein, E. G.; Holden, Z. C.; Jagau, T.-C.; Ji, H.; Kaduk, B.; Khistyayev, K.; Kim, J.; Kim, J.; King, R. A.; Klunzinger, P.; Kosonkov, D.; Kowalczyk, T.; Krauter, C. M.; Lao, K. U.; Laurent, A. D.; Lawler, K. V.; Levchenko, S. V.; Lin, C. Y.; Liu, F.; Livshits, E.; Lochan, R. C.; Luenser, A.; Manohar, P.; Manzer, S. F.; Mao, S.-P.; Mardirossian, N.; Marenich, A. V.; Maurer, S. A.; Mayhall, N. J.; Neuscammann, E.; Oana, C. M.; Olivares-Amaya, R.; O'Neill, D. P.; Parkhill, J. A.; Perrine, T. M.; Peverati, R.; Prociuk, A.; Rehn, D. R.; Rosta, E.; Russ, N. J.; Sharada, S. M.; Sharma, S.; Small, D. W.; Sodt, A.; Stein, T.; Stück, D.; Su, Y.-C.; Thom, A. J. W.; Tsuchimochi, T.; Vanovschi, V.; Vogt, L.; Vydrov, O.; Wang, T.; Watson, M. A.; Wenzel, J.; White, A.; Williams, C. F.; Yang, J.; Yeganeh, S.; Yost, S. R.; You, Z.-Q.; Zhang, I. Y.; Zhang, X.; Zhao, Y.; Brooks, B. R.; Chan, G. K. L.; Chipman, D. M.; Cramer, C. J.; Goddard, W. A.; Gordon, M. S.; Hehre, W. J.; Klamt, A.; Schaefer, H. F.; Schmidt, M. W.; Sherrill, C. D.; Truhlar, D. G.; Warshel, A.; Xu, X.; Aspuru-Guzik, A.; Baer, R.; Bell, A. T.; Besley, N. A.; Chai, J.-D.; Dreuw, A.; Dunietz, B. D.; Furlani, T. R.; Gwaltney, S.

R.; Hsu, C.-P.; Jung, Y.; Kong, J.; Lambrecht, D. S.; Liang, W.; Ochsenfeld, C.; Rassolov, V. A.; Slipchenko, L. V.; Subotnik, J. E.; Van Voorhis, T.; Herbert, J. M.; Krylov, A. I.; Gill, P. M. W.; Head-Gordon, M. *Mol. Phys.* **2015**, *113*, 184–215.

(34) Hehre, W. J.; Ditchfield, R.; Pople, J. A. *J. Chem. Phys.* **1972**, *56*, 2257.

(35) Hay, P. J.; Wadt, W. *J. Chem. Phys.* **1985**, *82*, 270–283.

(36) Dunning, T. H., Jr. *J. Chem. Phys.* **1989**, *90*, 1007–1023.

(37) Baik, M.-H.; Friesner, R. A. *J. Phys. Chem. A* **2002**, *106*, 7407–7412.

(38) Wohlfarth, C. Static Dielectric Constants of Pure Liquids and Binary Liquid Mixtures. In *Supplement to IV/6*; Lechner, M. D., Ed.; Springer Berlin Heidelberg: Berlin, Heidelberg, 2008; pp 67–68.

(39) CCCBDB listing of precalculated vibrational scaling factors; <https://cccbdb.nist.gov/vibscalejust.asp> (Accessed 2 Mar. 2018).

(40) *Chemissian v4.52*; www.chemissian.com (accessed Nov 02, 2017).

(41) Goldman, A. S.; Krogh-Jespersen, K. *J. Am. Chem. Soc.* **1996**, *118*, 12159–12166.

(42) Ehlers, A. W.; Ruiz-Morales, Y.; Baerends, E. J.; Ziegler, T. *Inorg. Chem.* **1997**, *36*, 5031–5036.

(43) Willner, H.; Aubke, F. *Angew. Chem., Int. Ed. Engl.* **1997**, *36*, 2402–2425.

(44) Niu, S.; Thomson, L. M.; Hall, M. B. *J. Am. Chem. Soc.* **1999**, *121*, 4000–4007.

(45) Xu, Q. *Coord. Chem. Rev.* **2002**, *231*, 83–108.

(46) Borden, W. T. *Chem. Rev.* **1989**, *89* (5), 1095–1109.

(47) (a) Gleiter, R.; Bleiholder, C.; Rominger, F. *Organometallics* **2007**, *26*, 4850–4859. (b) Bleiholder, C.; Rominger, F.; Gleiter, R. *Organometallics* **2009**, *28*, 1014–1017.

(48) Volland, M. A. O.; Kudis, S.; Helmchen, G.; Hyla-Kryspin, I.; Rominger, F.; Gleiter, R. *Organometallics* **2001**, *20*, 227–230.

(49) Chong, D.; Laws, D. R.; Nafady, A.; Costa, P. J.; Rheingold, A. L.; Calhorda, M. J.; Geiger, W. E. *J. Am. Chem. Soc.* **2008**, *130*, 2692–2073.

(50) Orpen, A. G.; Connelly, N. G. *Organometallics* **1990**, *9*, 1206–1210.

(51) Therien, M. J.; Ni, C.-L.; Anson, F. C.; Osteryoung, J. G.; Trogler, W. C. *J. Am. Chem. Soc.* **1986**, *108*, 4037–4042.

(52) Basolo, F. *New J. Chem.* **1994**, *18*, 19–24.

(53) Geiger, W. E. *Organometallics* **2007**, *26*, 5738–5765.

(54) Camire Ohrenberg, N.; Paradee, L. M.; Dewitte, R. J., III; Chong, D.; Geiger, W. E. *Organometallics* **2010**, *29*, 3179–3186.

(55) Currents in the cyclic and linear scan voltammograms are proportional to the square root of the diffusion coefficient of the analyte. The diffusion coefficient of the triphenyl phosphite derivative is expected to be considerably lower than that of the tricarbonyl complex, owing to its higher molecular weight. For a discussion of how variations in molecular weight affect the diffusion coefficients in a family of molecules, see: Flanagan, J. B.; Margel, S.; Bard, A. J.; Anson, F. A. *J. Am. Chem. Soc.* **1978**, *100*, 4248–4253.

(56) In ref 21, the $E_{1/2}$ potential of **4** is given as 0.02 V vs SCE in methanol/[NBu₄][BF₄]. Conversion to the ferrocene potential is an estimate.

(57) Lever, A. B. P. *Inorg. Chem.* **1990**, *29*, 1271–1285.

(58) Atwood, C. G.; Geiger, W. E.; Bitterwolf, T. E. *J. Electroanal. Chem.* **1995**, *397*, 279–285.

(59) Giordano, P. J.; Wrighton, M. S. *Inorg. Chem.* **1977**, *16*, 160–166.